CHAPTER II

Thermo-Elastic Collector Plate Design

2.1 Introduction

The gains associated with solar thermal energy collectors are comparatively small in relation to the required capital investment, so it is vital to maximize conversion efficiency. A typical active solar hot water heating system has a collector through which a working fluid is pumped and a tank for water storage. In cold climates, a heat exchanger is typically placed between the collector and the tank so that antifreeze solution may be circulated in the collector, providing freeze protection to the system. However, the addition of a heat exchanger, reduces the collector's useful energy output. It would greatly increase the viability of solar energy as a water-heating alternative if the heat exchanger loss could be eliminated since the energy output would be greater and the capital investment would be smaller.

This chapter examines one proposed remedy to the heat exchanger energy loss problem. If the collector tubes were made of a material that allowed the working fluid to expand and contract, then freeze protection would be built into the system and the heat exchanger would be unnecessary. After a brief discussion of previous experiments in this area and a description of a standard collector configuration, various mathematical models of the expandable collector will be analyzed and compared.

2.2 Background

Before examining possibilities for remedying the heat exchanger penalty it is important to understand the circumstances under which the penalty is minimal and under what circumstances it becomes significant. Figure 2.2.1 shows the dependence of the annual solar fraction (the fraction of a heating load met by solar) on the effectiveness of the heat exchanger in the system. There is a great benefit to increasing the effectiveness of the heat exchanger if it is very low to begin with but the benefit decreases as the effectiveness increases.

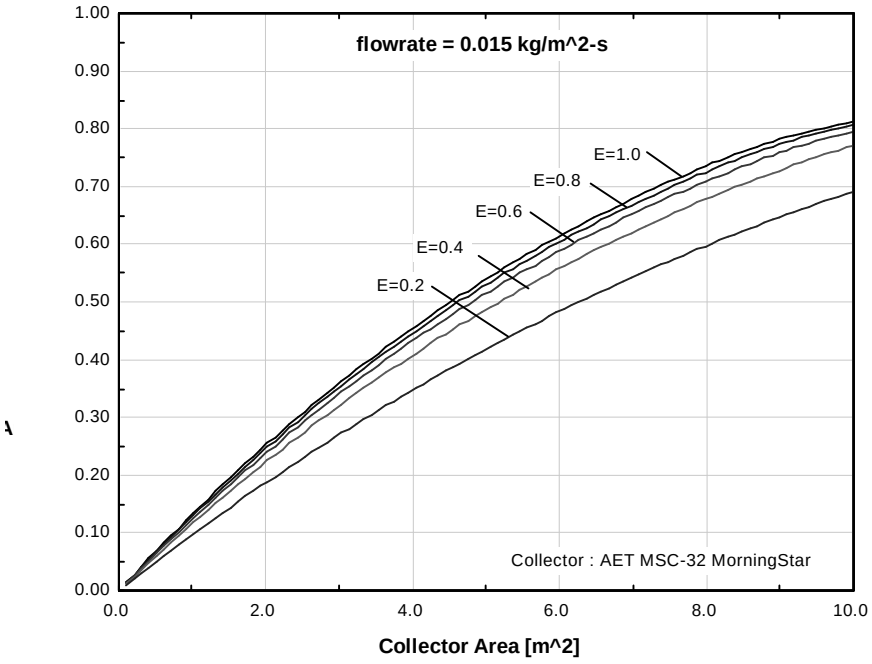

Figure 2.2.1: Heat Exchanger Penalty

One proposed remedy to the freezing problem is to make the collector tubes out of an elastic material that would allow the water to expand on freezing without damaging the

collector itself. A literature search has shown that this method has met with limited success. All of the work on the subject has been purely experimental. An experiment at the Solar Energy Research Institute evaluated water filled polybutylene piping under repeated freeze thaw cycles (Farrington, 1987). While the piping can withstand temperatures only to 93°C, it survived repeated freezing for 700 cycles before a crack appeared. Freezing problems were more common at the couplings between pipe sections.

Another experiment involved the manufacture of a carbon black reinforced cross-linked polyethylene collector whose absorber plate consisted of a 400-foot length of flat, spiraled tubing. Tube specimens were subjected to 100 freeze thaw cycles and, for some polyethylene formulations, they fared well (Bradley, 1977). It was found that the material had to be quite resilient (less reinforcement) because the stiffer formulations deformed plastically, creating ballooning problems at sections of the tubing where the wall was comparatively thin due to manufacturing imperfections. As water froze, stress concentrations occurred at these points and caused rupture. The reported $F_R(\tau\alpha)$ (intercept factor) for this collector was approximately 0.8 and the F_RU_L was 1.03 W/m^2-C. These numbers are somewhat suspect as the intercept efficiency is high and the loss coefficient is low even for a modern copper plate collector.

The standard flat-plate collector is made up of a series of parallel copper tubes separated by thin, copper or aluminum fins that run along the length of the tube. The bottom part of figure 2.2.2 shows the end view of one of these fin tube arrangements. Radiant energy incident on the fins is conducted towards the tubes where it is transferred

to a working fluid. Because the copper has a high thermal conductivity and because the fin thickness is small in comparison to its width, the transfer of energy to the water can be thought of as one-dimensional along the width of the fin and around the tube wall. In the analysis of this problem, two assumptions are made concerning temperatures. First, the temperature around the circumference of the tube is assumed to be constant. Second, there is a small increase in temperature along the length of the fin due to the fin material's finite heat transfer coefficient. A typical temperature profile is shown in figure 2.2.2.

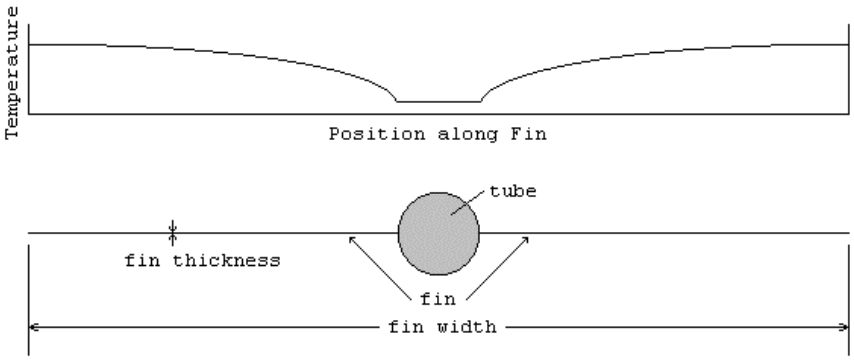

Figure 2.2.2: Temperature Distribution in a Copper Fin and Tube (End View)

In a regular elastic material, long chains of polymer are tangled together and attached to one another by crosslinks. The process of vulcanization makes use of sulfur atoms to crosslink polymer chains. Applying a force to a non-crosslinked polymer causes plastic deformation in the material. If, however, there are crosslinks, the polymer chains are brought back to their original shape after the force is removed. The problem with elastomers is that when heated, the crosslinks tend to break and the material deforms plastically. Thermo-elastomers, on the other hand do not rely upon crosslinks for their

elastic properties. Instead, the polymer chains are capped and attached to one another by rigid regions. Figure 2.2.3 shows a thermo-elastomer called styrene-butadiene in which butadiene chains, having a low glass transition temperature are rubbery at room temperature. Between these chains are rigid areas of high glass transition temperature styrene (Askeland, 1994).

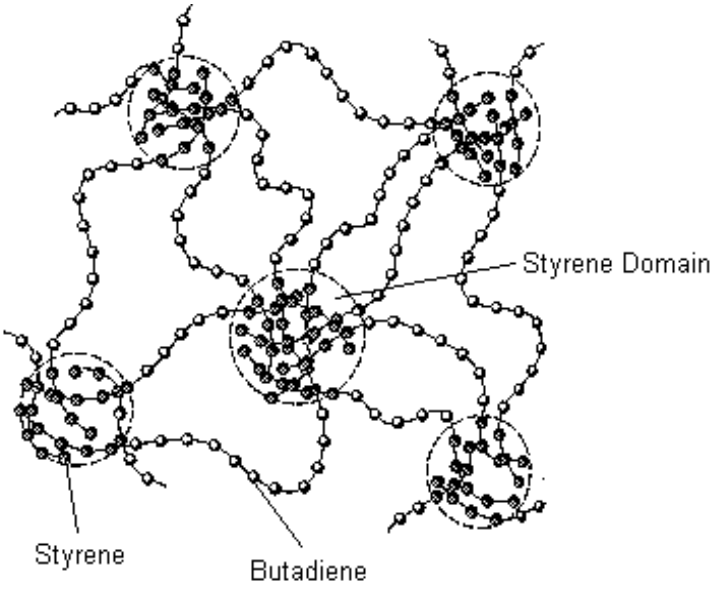

Figure 2.2.3: Molecular Structure of a Thermo-Elastomer

Unfortunately, along with their elastic properties, thermo-elastomers have low thermal conductivities meaning that energy incident on the fin would have a difficult time getting conducted to the fluid. Consequently, there would be significant temperature rise in the fins. To aid in the energy transfer along the fin and to prevent the high temperatures, a thermo-elastic collector would probably have short thick fins. For these reasons, neither the constant temperature around the tube assumption nor the one-dimensional heat transfer along the fin assumption holds true. In order to assess the idea

of a thermo-elastic collector, a one-dimensional model was created (Appendix A). This model allowed a temperature distribution along the circumference of the tube as well as along the length of the fin. The results of this model were validated by use of a finite element analysis program that modeled the problem in two dimensions.

2.3 Development of a One Dimensional Model

It is important to notice that the collector fin shown in figure 2.2.2 has an axis of symmetry about the center of the tube. The problem can therefore be broken up into three fins attached at a center point as shown in figure 2.3.1. The original fin has an energy input along its top face, and loses energy from both its top and its bottom faces. The second fin is a quarter of the circumference of the tube with a radiative input, convective loss on its top face, and a convective loss to the fluid on its back face. The third fin consists of the tube bottom quarter, with convective losses both to the environment off its back face and to the fluid.

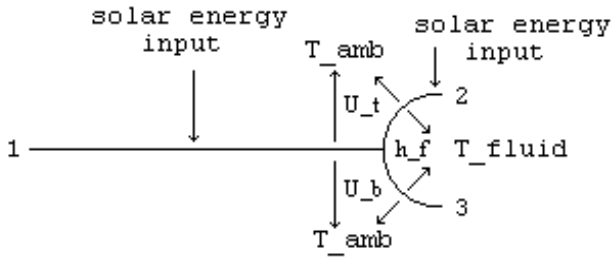

Figure 2.3.1: Energy Balance on Fins

In the one-dimensional analysis, the second and third fins were assumed to be straight so that the configuration was that of a T shape. The fact that only half the tube is being analyzed means that the ends of each fin can be assumed to be perfectly insulated (Figure 2.3.2).

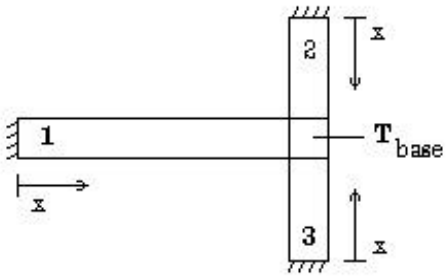

Figure 2.3.2: One-dimensional Model Configuration

In evaluating the amount of energy transferred to the working fluid, it was first necessary to find the temperature at the intersection of the three fins (labeled T_{base} in figure 2.3.2). Energy balances were performed on each of the three fins assuming that the free ends were perfectly insulated due to symmetry and that the point of intersection had a temperature of T_{base}. The energy balance for an element of length Δx of along fin 1, is given by equation 2.3.1.

$$S\Delta x - U_t \Delta x(T - T_{amb}) + (-k\,d\frac{dT}{dx}\Big|_x) - (-k\,d\frac{dT}{dx}\Big|_{x+\Delta x}) - U_b \Delta x(T - T_{amb}) = 0 \tag{2.3.1}$$

Where S is the incident radiation per unit area, U_t is the convective heat loss coefficient per unit area for the top of the fin, U_b is the heat loss coefficient for the back of the fin, k is the thermal conductivity of the fin material, δ is the thickness of the fin, and T is the local temperature of the element. The signs of each term are determined by the coordinate

system shown in figure 2.3.2. The energy balance can be rewritten as a differential equation by dividing equation 2.3.1 through by Δx and finding the limit as Δx approaches zero.

$$S-(U_t+U_b)(T-T_a)-k\,d\frac{dT}{dx}+k\,d\frac{dT}{dx}+k\,d\frac{d^2T}{dx^2}=0 \tag{2.3.2}$$

The equation can then be rewritten as

$$\frac{d^2T}{dx^2}=\frac{U_t+U_b}{k\,d}\left[T-T_a-\frac{S}{U_t+U_b}\right] \tag{2.3.3}$$

Two boundary conditions are used in solving the above equation. First, the base temperature must be known, and second, the derivative of temperature with respect to location is zero at the insulated end of the fin. (Equation 2.3.4)

$$T\Big|_{x=(W-D/2)}=T_b \qquad\qquad \frac{dT}{dx}\Big|_{x=0}=0 \tag{2.3.4}$$

In order to simplify the algebra, two variables are defined as shown in equation 2.3.5

$$m=\sqrt{\frac{U_t+U_b}{k\,d}} \qquad\qquad \Psi=T-T_a-\frac{S}{U_t+U_b} \tag{2.3.5}$$

Equation 2.3.2 can thus be rewritten as

$$\frac{d^2\Psi}{dx^2}-m^2\Psi=0 \tag{2.3.6}$$

Having the boundary conditions

$$\left.\frac{d\Psi}{dx}\right|_{x=0} = 0 \qquad \Psi|_{x=(W-D/2)} = T_b - T_a - \frac{S}{U_t + U_b} \tag{2.3.7}$$

The general solution to the differential equation is

$$\Psi = C_1 \sinh(mx) + C_2 \cosh(mx) \tag{2.3.8}$$

Constants C_1 and C_2 are found by substitution of the boundary conditions. The resulting solution is

$$\frac{T - T_a - \frac{S}{U_t + U_b}}{T_b - T_a - \frac{S}{U_t + U_b}} = \frac{\cosh(mx)}{\cosh\left(m\frac{W-D}{2}\right)} \tag{2.3.9}$$

Since the energy balances of each fin differ slightly, the equations for Ψ and m are also different. Equation 2.3.10 shows the energy balance on fin 2.

$$S\Delta x - U_t \Delta x(T - T_a) - h_f(T - T_f) + \left(-k\,d\left.\frac{dT}{dx}\right|_x\right) - \left(-k\,d\left.\frac{dT}{dx}\right|_{x+\Delta x}\right) - U_b \Delta x(T - T_a) = 0 \tag{2.3.10}$$

Ψ and m for fin 2 are given in equation 2.3.11.

$$m_t = \sqrt{\frac{U_t + h_f}{k\,d_t}} \qquad \Psi = T - \frac{1}{U_t + h_f}\left(U_t T_a + h_f T_f + S\right) \tag{2.3.11}$$

And the solution is given in 2.3.12.

$$\frac{T_{top}-\left[\left(\frac{1}{U_t+h_f}\right)\left(U_t T_a+h_f T_f+S\right)\right]}{T_b-\left[\left(\frac{1}{U_t+h_f}\right)\left(U_t T_a+h_f T_f+S\right)\right]}=\frac{\cosh\left(m_t x_t\right)}{\cosh\left[m_t p\frac{D}{4}\right]} \tag{2.3.12}$$

The energy balance for fin 3 is much the same as that of fin 2 except that there is no solar energy input.

$$-U_t\Delta x\left(T-T_a\right)-h_f\left(T-T_f\right)+\left(-k\,d\left.\frac{dT}{dx}\right|_x\right)-\left(-k\,d\left.\frac{dT}{dx}\right|_{x+\Delta x}\right)-U_b\Delta x\left(T-T_a\right)=0 \tag{2.3.13}$$

The equations for Ψ and m follow.

$$m_b=\sqrt{\frac{U_b+h_f}{k\,d_b}} \qquad\qquad \Psi=T-\frac{1}{U_b+h_f}\left(U_b T_a+h_f T_f\right) \tag{2.3.14}$$

Which generates the solution

$$\frac{T_{bot}-\left[\left(\frac{1}{U_b+h_f}\right)\left(U_b T_a+h_f T_f\right)\right]}{T_b-\left[\left(\frac{1}{U_b+h_f}\right)\left(U_b T_a+h_f T_f\right)\right]}=\frac{\cosh\left(m_b x_b\right)}{\cosh\left[m_b p\frac{D}{4}\right]} \tag{2.3.15}$$

Equations 2.3.9, 2.3.12, and 2.3.15 provide the local temperature as a function of distance along each fin. However, the base temperature where the fins meet must also be known. The energy conducted to the base point can be found by evaluating Fourier's law at the base point where x = L on fin 1 and where x = πD/4 on fins 2 and 3.

$$q_{fin} = -k\,d\left.\frac{dT}{dx}\right|_{x=L}$$

(2.3.16)

The resulting equations for each fin are shown in equations 2.3.17 through 2.3.19. Q_{fin} is the total energy transferred to the base point from the fin one.

$$q_{fin} = -m_f\,k\,d_t\left[T_b - T_a - \left(\frac{S}{U_t + U_b}\right)\right]\tanh\left[m_f\left(\frac{W-D}{2}\right)\right]$$

$$\text{where} \quad m_f = \sqrt{\frac{U_t + U_b}{k\,d_t}} \qquad (2.3.17)$$

In the above equation, W is the fin width, D is the diameter of the tube as defined in figure 2.2.1, and T_b is the base temperature. Q_{top} is the energy transferred to the base point from the top quarter circumference of the tube and h_f is the convective heat transfer coefficient between the tube wall and the working fluid.

$$q_{top} = -m_t\,k\,d_t\left[T_b - \left[\frac{1}{U_t + h_f}\right](U_t T_a + h_f T_f + S)\right]\tanh\left[m_t\,p\,\frac{D}{4}\right]$$

$$\text{where} \quad m_t = \sqrt{\frac{U_t + h_f}{k\,d_t}}$$

(2.3.18)

Q_bot is the energy transferred to the base point from the bottom half of the tube.

$$q_{bot} = -m_b\,k\,d_b\left[T_b - \left[\frac{1}{U_b + h_f}\right]\left(U_b T_a + h_f T_f\right)\right]\tanh\left[m_b\,p\,\frac{D}{4}\right]$$

$$\text{where} \quad m_b = \sqrt{\frac{U_b + h_f}{k\,d_b}}$$

(2.3.19)

There is also an amount of energy that flows directly from the base point to the water.

$$q_{end} = h_f \, d_f \, (T_b - T_f) \tag{2.3.20}$$

To solve for the temperature at the intersection point, it is necessary to perform an energy balance on the base point itself.

$$q_{fin} + q_{top} + q_{bot} = q_{end} \tag{2.3.21}$$

The desired result is an estimate of the energy transferred to the water from the fin so it is necessary to integrate the energy flow along the length of the tube top and bottom. Since the tube was broken at its axis of symmetry for this analysis, the length of integration would normally be one quarter of the tube circumference for each of the top and bottom portions of the tube. Equation 2.3.22 is used twice, once for fin 2, and again for fin 3. The local temperatures are determined by evaluating equations 2.3.9, 2.3.12 and 2.3.15.

$$q_{water} = \int_0^{x\max} h_f \, (T - T_f) \, dx \tag{2.3.22}$$

The energy transferred to the water is the sum of q_{water} for the top portion of the tube, q_{water} for the bottom portion of the tube and q_{end} (figure 2.3.3)

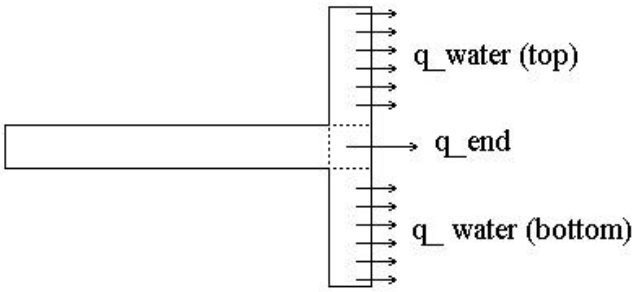

Figure 2.3.3: Energy Transferred to Water

In the next section, various fin tube configurations will be analyzed. In these configurations, the thickness of the tube wall and the thickness of the fin will be varied. There are a few complications in analyzing certain fin tube configurations. In evaluating the integral in equation 2.3.22, a length of integration must be chosen. As previously mentioned, when the tube wall thickness is small in relation to the diameter such as in the standard configuration, then a quarter of the circumference (the length of fin 2 or fin 3) is used. However, when the tube wall is thick then the base point is no longer a point and has some area associated with it. Thus there are a number of different tube dimensions that can be used in evaluating the circumference and therefore the integration length. Energy is collected along the outer surface and is transferred to the water along the inner surface. These surfaces can differ significantly in length. When evaluating heat transfer in such thick walled cylinder situations, an equivalent diameter is used that may be half or two thirds of the way through the cylinder wall. In this case, however, there is the added complication of fin 1 to deal with. When fin 1 is thick, the base point becomes large and the equivalent tube circumference is further reduced. To choose the integration length, the method illustrated in figure 2.3.4 was used.

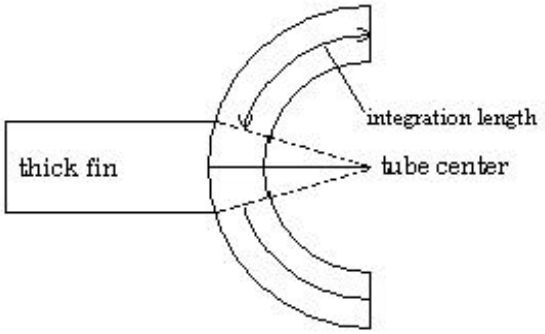

Figure 2.3.4: Reduction in Integration Length due to Fin and Tube Thickness

Radial lines are drawn from the center of the tube to the points where fin one meets either fin two or fin three. The trapezoidal area where the three fins meet is assumed to be the base point and the integration length is taken as the remaining length of the centerline of either fin two or three.

The performance prediction results of the one-dimensional analysis appeared to be reasonable. But lacking experimental data for comparison, they cannot be validated. Two assumptions had been made that needed validation. First, does the one-dimensional model approach reality or are the two-dimensional heat transfer effects important? Second, the choice of integration length was somewhat arbitrary and needed to be justified by a more realistic model such as a finite element analysis.

2.4 A Two Dimensional Model: Finite Element Analysis

In general, a one-dimensional model can be used in analyzing a fin if the thickness to length ratio is less than 0.1 (Holman, 1995). The initial results of the one-dimensional model showed that the collector would have tubes separated by a fin 1 cm wide and 0.5 cm thick, a configuration which does not meet the above criteria. Thus, two-dimensional effects are important. However, the desired end result of this analysis is an estimation of the amount of energy transferred to the water. Thus if the one-dimensional model and a two-dimensional model agree, then the simpler of the two may be used. Since creating two-dimensional models is time consuming, while one-dimensional models can be created by simply changing the input values to a few equations, it would be convenient if the one-dimensional model were useable. Using finite element heat transfer analysis software, FEHT (Klein, 1990), collector configurations similar to those analyzed using the one-dimensional model were run in an effort to determine whether these two dimensional effects were important. The temperature distribution shown in figure 2.4.1 definitely shows some two-dimensional effects especially near the end of fin one, furthest from the intersection point. Furthermore, there are significant temperature distributions around the circumference of the tube. The lines in the figure are lines of constant temperature over a range of 38°C to 122°C. The effect of the low thermal conductivity is evident here; a standard copper collector has a much smaller temperature rise along the length of the fins.

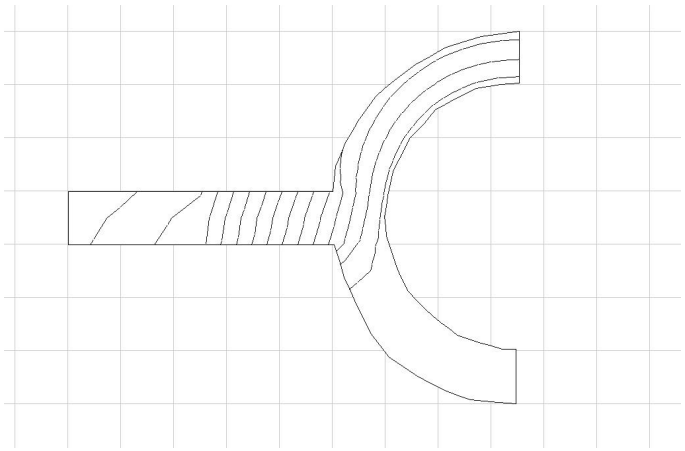

Figure 2.4.1: Temperature Distribution

In an effort to separate the low thermal conductivity contribution to the two-dimensional temperature distribution from the thick fin contribution, figures 2.4.2(a-d) show the same plate geometry with various thermal conductivities.

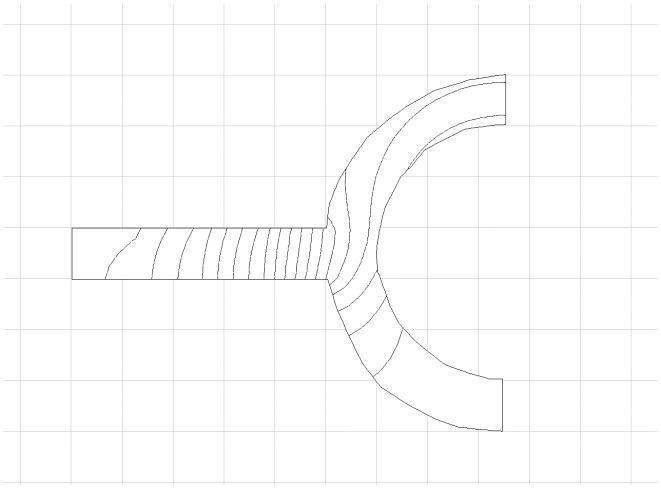

Figure 2.4.2a: Temperature Distribution with k = 1 W/m-K
Temperature Rise along fin: 26^{o}C

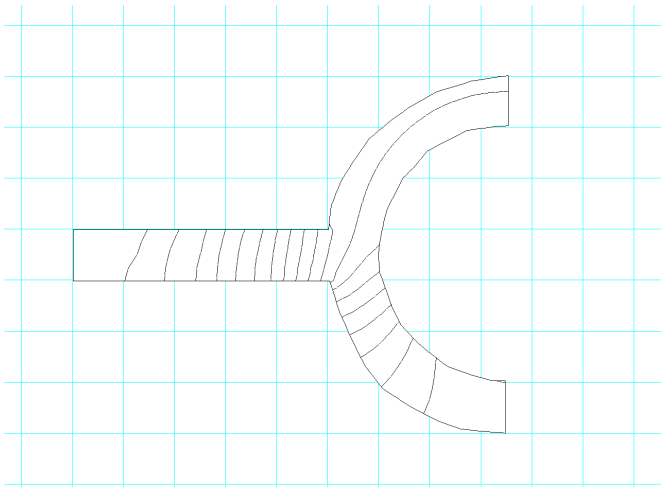

Figure 2.4.2b: Temperature Distribution with k = 10 W/m-K
Temperature Rise along fin: 5^{o}C

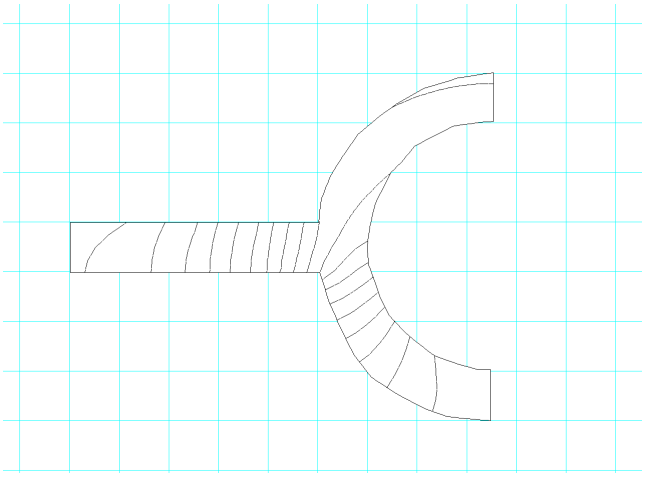

Figure 2.4.2c: Temperature Distribution with k = 400 W/m-K
Temperature Rise along fin: 0.5^{o}C

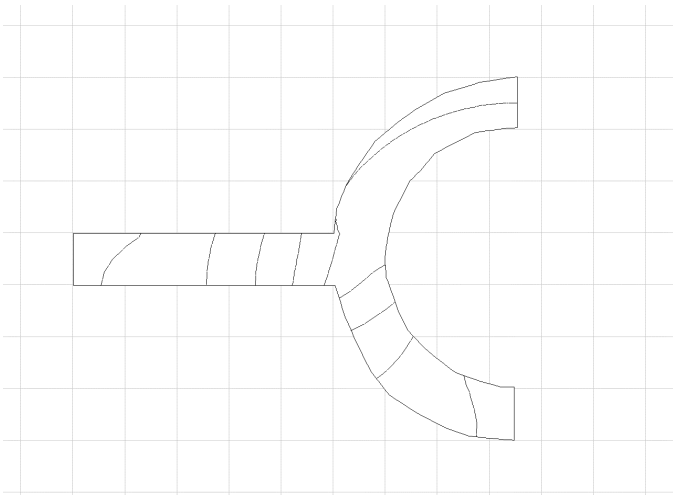

Figure 2.4.2d: Temperature Distribution with k = ¥ W/m-K
Temperature Rise along fin: 0.1°C

Evidently, the thickness of the fin does contribute to the two-dimensionality of the results. However, a high thermal conductivity means that the temperature difference through the thickness of the fin is miniscule that the two-dimensional effects do not matter. Another problem becomes apparent through these figures. Because of the thickness of the tube wall, the temperature distribution is in the wrong direction for a fin and therefore cannot be analyzed as such. Since the temperature profile is parallel to the length of the fin, it must be analyzed as a wall. The problem is described in greater detail in section 2.8

2.5 Comparison of One and Two Dimensional Models

Twenty-seven models were analyzed using both the one and two-dimensional models with fin and tube wall thicknesses varying between 0.1 and 0.9 centimeters. In all cases, the fin was one centimeter long. The fin length was chosen to provide some surface area for incident radiation while limiting the temperature rise along the fin. The solar input

was 1000 W/m^2-K, the plate top convective heat loss coefficient was 7 W/m^2 and the back loss coefficient was 1 W/m^2-K. These numbers are typical for a single cover collector with a non selective surface plate and an insulated back. The tube inside diameter was always 1 centimeter. The results for the models are encouraging. For the range between 0.1 and 0.5 cm thickness, there is less than 10% difference in the prediction of energy transferred to the water between the two models (Figure 2.5.1). Predictably the agreement is better when the tube wall thickness and the fin thickness are nearly equal (ratio = 1) and becomes worse as one or the other gets comparatively thicker.

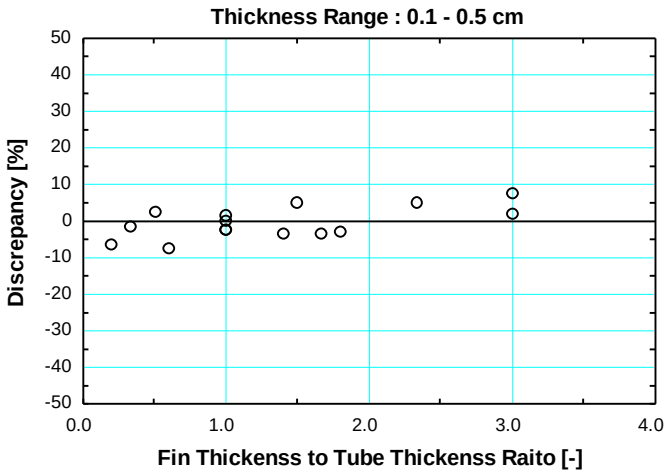

Figure 2.5.1: Comparison between One and Two-Dimensional Models (0.1 - 0.5 cm)

As thicker fins are added to the evaluation, results between the one and two-dimensional models diverge further, even when the fin and tube thicknesses are equal (figure 2.5.2)

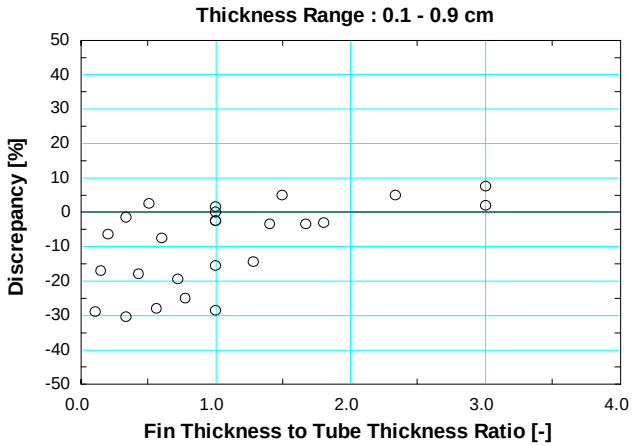

Figure 2.5.2: Comparison between One and Two Dimensional Models (0.1 - 0.9 cm)

2.6 Obtaining Useful Design Parameters from the Model

Once the one-dimensional model had been validated for thicknesses ranging from 0.1 to 0.5 cm, it was possible to use the model in predicting the performance of a thermo-elastic collector. Collector performance can be described by equation 2.6.1 (Duffie and Beckman, 1991).

$$Q_u = A_c F_R (I_T ta - U_L (T_i - T_a)) \tag{2.6.1}$$

In the above equation, F_R is the collector heat removal factor, $\tau\alpha$ is the transmitance absorptance product, and U_L is the loss coefficient. The one-dimensional model was used to determine values of F_R for various possible collector designs. Both F` and F_R vary between 0 and 1.

The first step in estimating F_R is to determine F', the collector efficiency factor. F' is the amount of energy transferred to the fluid divided by the amount of energy incident

on the collector surface. The plot in figure 2.6.1 shows the F' curves for various collector configurations created using the one dimensional model. In all of these cases, the tube diameter was 1 centimeter, collector losses (U_L) were 8 W/m^{2}K, and the tube wall thickness was 3 mm. Each curve corresponds to a different kδ product (fin thickness times thermal conductivity).

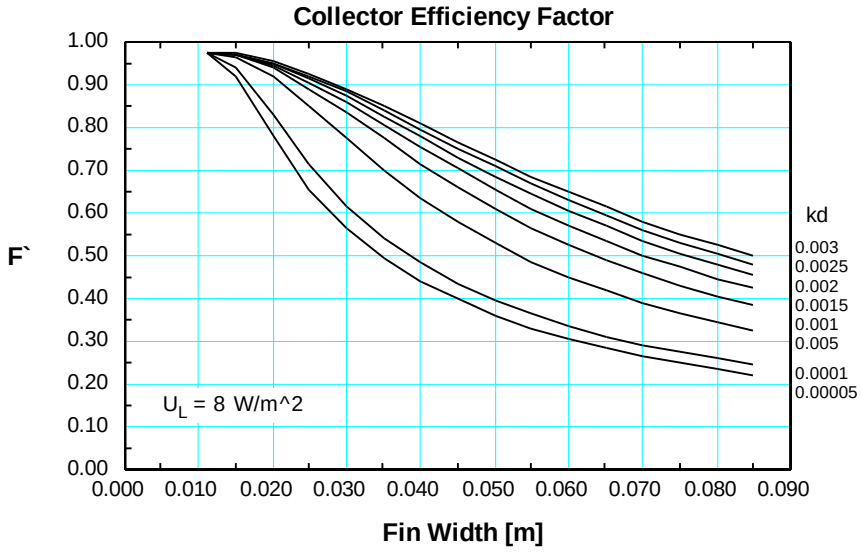

Figure 2.6.1: Collector Efficiency Factor for a Range of k d

The collector heat removal factor (F_R) is defined as follows (Duffie and Beckman, 1991).

$$F_R = \frac{\dot{m} C_p}{A_c (U_t + U_b)} \left[1 - \exp\left(\frac{-A_c F'(U_t + U_b)}{\dot{m} C_p} \right) \right] \qquad (2.6.2)$$

Equation 2.6.2 assumes that the specific heat (C_p), collector efficiency factor (F'), top losses (U_t), and back losses (U_b) are fairly constant over the operating temperature range (Duffie and Beckman, 1991).

The estimation of F_R requires the mass flow rate of the fluid which figures into the internal convective heat transfer coefficient through a Nusselt number and Reynolds number correlation (Equation 2.6.3).

$$h_f = \frac{Nuk}{D}$$

$$Nu = 3.66 \qquad \text{for laminar flow} \qquad (2.6.3)$$

$$Nu = 0.023 \mathrm{Re}^{4/5} \mathrm{Pr}^{1/3} \quad \text{for turbulent flow}$$

In figure 2.6.2, the jump in F_R seen at a mass flow rate per area of 0.005 to 0.0055 is a result of the change from laminar to turbulent flow inside the tubes. It should be noted here that the graph in figure 10 is for a fin width of three centimeters. As W decreases, the effect of the $k\delta$ product is a far less pronounced. The lower $k\delta$ curves are shifted upwards while the higher $k\delta$ curves remain essentially unchanged.

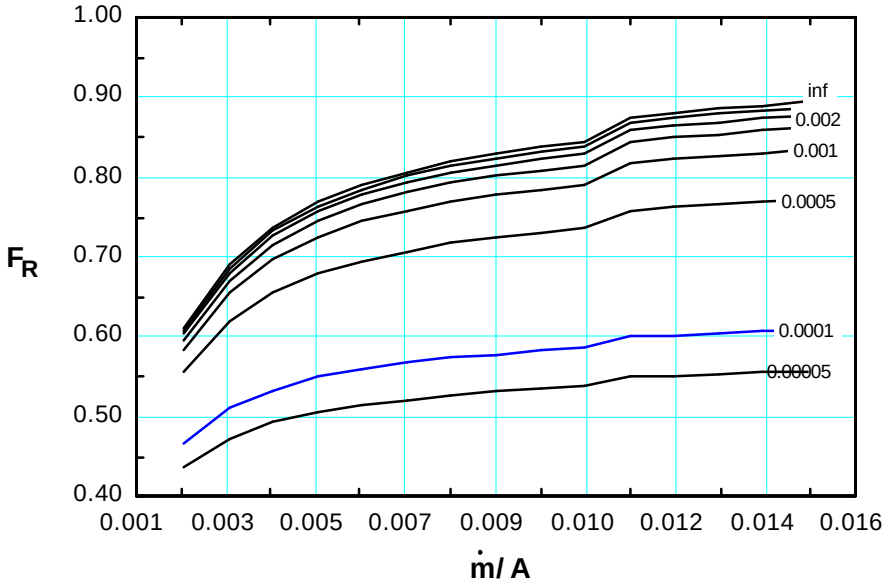

Figure 2.6.2: Collector Heat Removal Factor for a Range of k d

As a final check of model validity, a copper plate collector with typical dimensions was analyzed using both the one-dimensional model developed in section 2.3 and the accepted equations as presented by Duffie and Beckman (1991). The plot of F' for a copper collector using both the one-dimensional model and the standard design equation appears in figure 2.6.3.

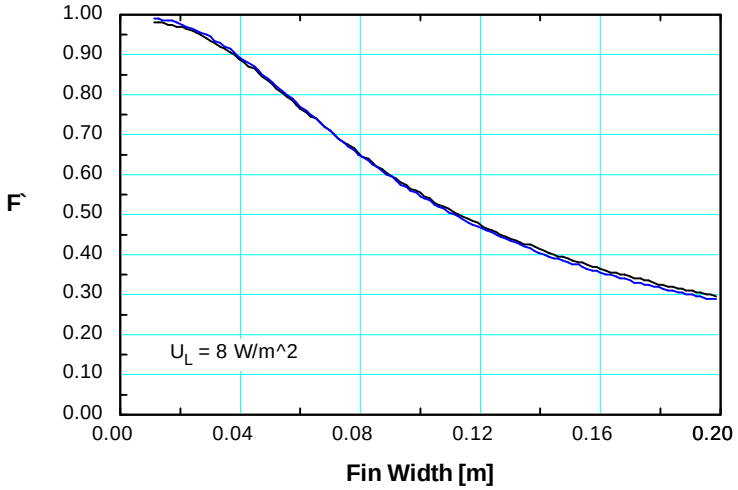

Figure 2.6.3: Model Verification for Standard Configuration

2.7 Designing a Thermo-Elastic Collector

With the one-dimensional model, it is possible to choose a reasonable design for a thermo-elastic collector. The restriction imposed by the use of the one-dimensional model is that the thickness of the plate and tube can be no greater than half a centimeter. Furthermore, the predicted F` and F_R values will be most accurate if the ratio of fin thickness to tube wall thickness is nearly unity. The end result of this design will be a comparison between the energy performance of the thermo-elastic collector and a standard copper collector. A useful indicator is the amount of thermo-elastic plate area required to match the amount of energy delivered by a standard copper collector. The solar simulation program *f*-Chart (Klein, 1993) was used in evaluating various designs.

F-Chart allows the user to specify various parameters concerning the collector and system, and then performs a thermal and an economic analysis, reporting monthly values.

As a preliminary comparison, a thermo-elastic collector of tube thickness 0.5 cm and fin thickness 0.5 cm was determined to have an F_R of 0.78 using the chart in figure 2.6.2. The mass flow rate was chosen to be 0.02 l/m^{2}s. Using information from Duffie and Beckman (1991), a $\tau\alpha$ product of 0.7 and a U_L value of 8 W/m^2 were chosen to be representative of a non selective surface material. The resulting thermal analysis was compared to the results of a standard American Energy Technologies collector Model AE-21 (SRCC, 1994). The relevant geometric data for the two collectors is shown below in Table 2.7.1.

Table 2.7.1: Collector Geometries

	AET Model AE-21 Copper Collector	Thermo-Elastic Collector
m_dot (kg/s m^2)	0.02	0.02
U_L (W/m^2)	not reported individually	8
$\tau\ \alpha$	not reported individually	0.75
F_R	not reported individually	0.78
F_R ($\tau\ \alpha$)	0.674	0.59
$F_R\ U_L$ (W/m^{2}C)	4.25	6.24

The tube diameter was chosen to be 1 centimeter. Care must be taken in choosing a tube diameter and wall thickness not to exceed the maximum hoop strength of the material. The hoop strength is determined as the maximum allowable stress (force/area) that can be internally applied to a thin walled pressure vessel made of the material without worry of material failure. For example cross-linked polyethylene can withstand a hoop stress of 241 psi. Equation 2.7.1 can be used to determine the maximum tube diameter for a given wall thickness (Beer and Johnston, 1992).

$$H = \frac{p(D-t)}{2t} \qquad (2.7.1)$$

H is the hoop stress, p is the internal hydrostatic pressure, D is the outside diameter of the tube and t is the wall thickness.

The comparison showed that, as expected, the thermo-elastic collector did not perform as well per unit area as the standard copper collector. Consequently, the aperture area of the thermo-elastic collector was increased until its annual solar fraction was equal to that of the copper collector.

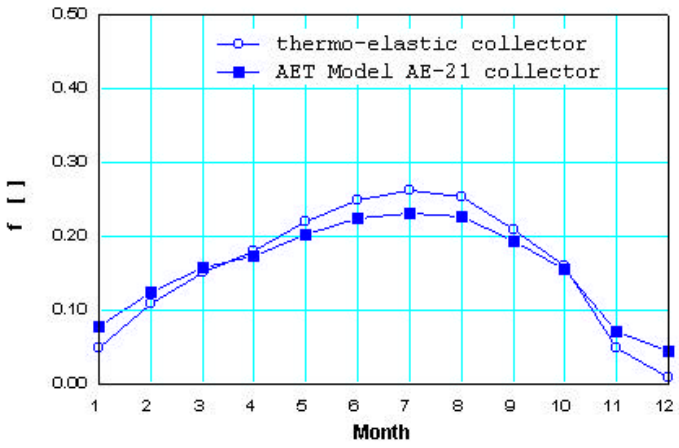

Figure 2.7.1: Monthly Solar Fraction for 2.6 m^2 Thermo-Elastic Versus 1.76 m^2 Model AE-21 Collector

The increase of area necessary to achieve a standard collector's energy output was chosen as a method of assessing the performance of the thermo-elastic collector. The AET collector had an aperture area of 1.76 m^2 that corresponded to an annual solar fraction of 0.156. The low solar fraction is due to only one collector panel being used in

the system. With the same aperture area, the thermo-elastic collector has a solar fraction of 0.109. An aperture area of 2.6 m^2 is needed to achieve a solar fraction of 0.156.

In can be seen from figure 2.7.1 that although the annual solar fraction is the same for the two collector types (0.157), that the thermo-elastic collector works better during the summer months (from an energy standpoint) and not as well during the winter. It must be kept in mind that this *f*-Chart analysis is purely thermal and does not take into account any benefits of freeze protection or reduced cost that a thermo-elastic collector might also include. It may appear odd that the plots of solar fraction cross when the thermo-elastic collector has both a lower intercept efficiency and a higher loss coefficient. However, it must be kept in mind that each plot was generated separately and that the collector areas were subsequently altered to obtain the same overall solar fraction. Were it not for the different areas the thermo-elastic collector plot would be almost coincident with the ordinate axis.

There are a number of points that have not been studied in this analysis, which are important to the design of a freeze tolerant collector. No work has been done in this analysis on material properties. In order to build a thermo-elastic collector, a material would have to be chosen that is able to withstand high temperature and high pressure without ballooning. According to Bradley (1977) carbon black reinforced cross-linked polyethylene is a promising alternative. His analysis goes into a fair amount of detail concerning the doping of polyethylene to obtain desired material properties. Furthermore, the header and footer of the collector pose a problem and need to be designed with a

freeze protection scheme of their own because forming ice could crack them or damage the joints between header and riser. A significant number of the failures mentioned in both the Farrington (1987) and the Bradley (1977) experiments were caused by a compression fitting working its way loose during repeated freeze thaw cycles.

2.8 Further Research

To be honest, there are a lot of gaps in the thermo-elastic collector analysis. A one-dimensional model was sought in order to speed up the design process simply because two dimensional models are time consuming to create; each new configuration needs to be redrawn and redefined completely from scratch. But since the conclusion of the design work has been that the tube walls need to be thick in order to provide structural integrity to the collector plate, the problem is without a doubt, two-dimensional. This is not to say that the work to date is invalid. Collectors can be designed from one-dimensional model equations as long as they have nearly the same geometries as those studied here (~1 cm fins and ~1 cm diameter tubes). Furthermore the research to date has proven that thermo-elastic collectors are a viable alternative and bear further investigation.

The next thing that needs to happen if thermo-elastic collectors are to be pursued is to create a method of predicting F' using a two-dimensional model. Since F' is simply the ratio of energy in to energy out, it is an easy procedure of summing the total energy flow into the top of the collector and summing the total energy flow into the fluid. Given F', a designer could then predict F_R and use it in equation 2.6.1 as before. Then a

prototype needs to be built in order to assess whether the fin separated tube design is best. It may well be that two thermo-elastic plates separated by vertical thermo-elastic risers as shown in figure 2.7.2 would be a simpler and more efficient collector.

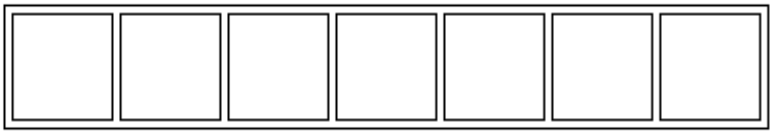

Figure 2.7.2: Square Tube Thermo-Elastic Collector Plate Design

2.9 Conclusions

A one dimensional model of a low thermal conductivity collector plate was developed in order to assess the possibility of providing a fail safe, built in freeze protection scheme. Because preliminary results indicated that short, thick fins would be desirable, two dimensional heat conduction effects were examined. A series of two-dimensional models were developed and results were compared to those of the single dimensional model. The models give comparable results for fin and tube thicknesses under 0.5 centimeters. Results are further improved if the fin and tube thicknesses are nearly the same.

The one-dimensional model was then used to provide design tools from which a collector geometry and mass flow rate can be chosen. Standard collector performance measures such as the collector efficiency factor and the heat removal factor were developed and used to design a thermo-elastic collector plate. Because of its low thermal conductivity, the thermo-elastic collector did not perform as well as a standard copper

plate collector. Thus, the aperture area was increased until a similar performance was achieved. To provide the same amount of energy on an annual basis, the thermo-elastic collector must be approximately 1.5 times as large as a standard collector must. Increasing the area will increase the amount of material required to build the collector. However, the manufacture of a copper collector involves bending a copper sheet around the tubes and then braising or welding the tubes into place to provide a good thermal bond. The thermo-elastic collector plate could be extruded in a single sheet, possibly significantly decreasing the manufacturing cost.

The suggested design of a thermo-elastic plate collector is that of one centimeter tubes with half centimeter thick walls separated by fins that are one centimeter long and again half a centimeter thick. The thickness of the plate gives a higher $k\delta$ product in figure 9 meaning that the collector efficiency is less dependent on tube spacing. Next, a flow rate of 0.02 l/m^2-s was chosen to give a high collector heat removal factor. With this configuration, an area 1.5 times greater than a typical copper collector will give comparable annual performance.